ARTICLE

OBC
www.rsc.org/obc

Substituent effects and the role of negative hyperconjugation in siloxycarbene rearrangements†

Paul G. Loncke‡ and Gilles H. Peslherbe*

Centre for Research in Molecular Modeling and Department of Chemistry and Biochemistry, Concordia University, 7141 Sherbrooke Street West, Montréal, Québec, Canada H4B 1R6. E-mail: ghp@alcor.concordia.ca; Fax: +1 (514) 848-2868; Tel: +1 (514) 848-2424 ext. 3335

Received 18th October 2004, Accepted 19th April 2005
First published as an Advance Article on the web 9th May 2005

Substituent effects and the role of negative hyperconjugation in 1,2-silyl migration and decarbonylation of methoxy(substituted-siloxy)carbenes have been investigated using quantum chemical calculations and natural bond orbital analysis. It has been found that σ-electron-withdrawing substituents generally lower the barriers for 1,2-silyl migration and decarbonylation, consistent with *symmetry-forbidden* concerted rearrangements involving intramolecular front-side nucleophilic attack by the carbene lone pair at silicon and by the methoxy oxygen at silicon, respectively. However, while good linear Hammett correlations are obtained for 1,2-silyl migration, those obtained for decarbonylation are poor. In addition, there appears to be a relationship between the extent of pertinent hyperconjugative interactions in the siloxycarbene conformers and the ease of intramolecular reactivity. As a matter of fact, the finding that 1,2-silyl migration is more favorable than decarbonylation seems to be primarily related to stronger negative hyperconjugation between the carbene lone pair and the O–Si antibonding orbital, compared to that between the methoxy oxygen n(σ) lone pair and the O–Si antibonding orbital. Moreover, the activation enthalpies for 1,2-silyl migration decrease linearly with stronger negative hyperconjugation, although no such correlation could be established for decarbonylation.

Introduction

We recently reported theoretical evidence that 1,2-silyl migration and decarbonylation of methoxy(siloxy)carbene are concerted rearrangements involving intramolecular *front-side* nucleophilic attack by the carbene lone pair at silicon and by the methoxy oxygen at silicon, respectively.[1–3] Since such rearrangements are *symmetry-forbidden*,[4–7] as evident from Scheme 1,[8] and quite rare, it is of interest to investigate substituent effects and the role of negative hyperconjugation in these intramolecular rearrangements.

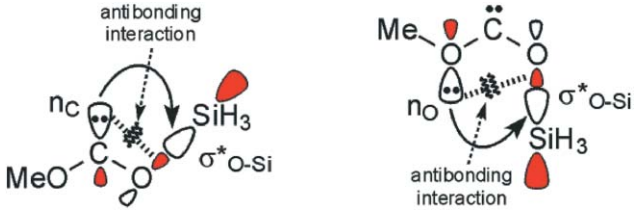

Scheme 1

Substituent effects are often assessed in terms of Hammett free-energy relationships. These relationships have provided valuable insight into the mechanisms of a number of singlet carbene reactions.[9–14] For example, Su and Thornton[9] and Liu and Bonneau[10] investigated substituent effects on 1,2-H shifts in *p*-substituted benzylmethylcarbenes and benzylchlorocarbenes, respectively. Logarithmic plots of rate constants, log *k*, *versus* substituent constants, σ_p and σ^+,[15,16] afforded Hammett reaction constants ρ close to -1.0,[17] consistent with the positive charge development at the migration origin that accompanies a hydride-like shift to the vacant carbene p orbital. Similarly, Moss *et al.* investigated 1,2-benzoyl migrations in a number of *p*-substituted benzoyloxyphenylcarbenes.[11] A Hammett plot of log *k* *versus* σ_p yielded a ρ value of -0.96,[17] consistent with nucleophilic attack by the carbene lone pair at the acyl carbon. Apparently, π-electron-donating substituents stabilize the acyl moiety in the transition state as it migrates with cation-like character to the carbon lone pair.[18] A variant of the Hammett relationship known as the *dual-substituent-parameter* (DSP) *equation*,[19] has also been applied to studies of carbene reactivity.[13,14] For instance, Rondan *et al.*[13] and Moss[14] examined the dependence of carbene stabilization energies and the carbene selectivity index on σ^+_R and σ_I,[15,16] for cycloaddition reactions between singlet carbenes and alkenes. In both studies, the coefficients of σ^+_R and σ_I were negative and positive, respectively,[17] indicating that π-electron-donating and σ-electron-withdrawing substituents stabilize carbenes and increase their selectivity.

It is widely believed that hyperconjugation dictates which rearrangements predominate when multiple rearrangements of singlet carbenes are possible. For example, Nickon *et al.*,[20] Freeman *et al.*[21] and Kyba *et al.*[22] found that 1,2-H shifts in 2-norbornylidenes occur preferentially from the *exo* rather than the *endo* position. Similarly, Press and Shechter[23] and Kyba *et al.*[24,25] reported that 1,2-H shifts in cyclohexylidenes occur with a noticeable preference for *axial* migration over *equatorial* migration. The observed selectivities have been attributed to stronger hyperconjugation between the *exo* C–H bond and the vacant carbene p orbital in 2-norbornylidenes, and between the *axial* C–H bond and the vacant carbene p orbital in cyclohexylidenes. These findings are supported by *ab initio* calculations, which have revealed that the *exo* C–H bond is longer than the *endo* C–H bond in 2-norbornylidenes, and that the *axial* C–H bond is longer than its *equatorial* counterpart in cyclohexylidenes. It has also been reported that 1,2-H migrations in singlet alkylchlorocarbenes bearing β-electronegative substituents afford the thermodynamically less stable *Z*-alkene isomers as the major products over their *E*-alkene counterparts.[26–30] The observed *Z*-selectivity is believed

† Electronic supplementary information (ESI) available: Tables S1–S4 and Figs. S1–S37. See http://www.rsc.org/suppdata/ob/b4/b416058d/

‡ *Present address:* Department of Chemistry, McMaster University, Hamilton, Ontario, Canada L8S 4M1

DOI: 10.1039/b416058d

to be due to the fact that the *cis*-carbene conformers are more stable than the corresponding *trans*-carbene conformers.[26–32] Apparently, the geometry of the *cis*-carbene conformers allows maximum interaction, and hence negative hyperconjugation, between the carbene lone-pair orbital and the σ^*_{C-W} antibonding orbital (where W denotes the β-electronegative substituent), as the largest lobes of these orbitals are able to overlap.

In this article, we report results from our investigation of substituent effects and the role of negative hyperconjugation in 1,2-silyl migration and decarbonylation of methoxy(substituted-siloxy)carbenes, which afford methyl silylformates and methyl silyl ethers, respectively (*cf.* Scheme 2). We will first examine substituent effects on the geometries and the electronic structures of the siloxycarbene conformers, as well as the transition states for 1,2-silyl migration and decarbonylation. Afterwards, we will discuss substituent effects in terms of Hammett free-energy relationships and assess the role of negative hyperconjugation in these siloxycarbene rearrangements.

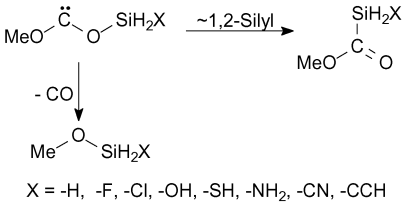

Scheme 2

Computational methods

Ab initio molecular orbital theory calculations at the Hartree–Fock (HF) and second-order Møller–Plesset (MP2) levels of theory,[33,34] and density functional theory calculations using the Becke three-parameter hybrid-exchange functional with the Lee–Yang–Parr correlation potential (B3LYP)[33,35,36] were performed with the 6-311+G(2d,p) basis set[33,34] using the Gaussian 98 suite of programs.[37] Siloxycarbenes are known to have large $S_0 \rightarrow T_1$ energy gaps, and calculations using the configuration interaction with single excitations (CIS) method confirm this fact. For instance, the CIS/6-31+G*//MP2/6-311+G(2d,p) $S_0 \rightarrow T_1$ energy gaps for the methoxy(siloxy)carbene conformers lie in the 55 to 57 kcal mol^{-1} range.[1] Similarly, the CIS/6-31+G*//MP2/6-311+G(2d,p) $S_0 \rightarrow T_1$ gaps of the transition states for 1,2-silyl migration and decarbonylation of methoxy(siloxy)carbene are 80.0 and 66.1 kcal mol^{-1}, respectively. Thus, since the triplet-state surface lies much higher in energy, only the singlet-state potential energy surface was considered in this work. Minimum-energy and transition-state geometries were obtained using the Berny algorithm[38] and the eigenvector following method,[39–41] respectively, and frequency calculations were performed for stationary-point characterization. Thermochemical data were obtained within the rigid-rotor harmonic-oscillator approximation based on standard statistical methods implemented in Gaussian 98.[42] Natural bond orbital (NBO) analysis[43] was carried out to determine atomic charges from natural population analysis (NPA) and to obtain stabilization energies due to hyperconjugation by either second-order perturbation-energy analysis or deletion of the appropriate Fock matrix elements, using the NBO program version 3.1[44] available in Gaussian 98. Atoms-in-molecules (AIM) analysis[45] was also carried out to determine bond critical point[46] (BCP) electronic densities $\rho_b(r)$ using the AIMPAC suite of programs.[47]

Results and discussion

Molecular geometry

Fig. 1 displays representative geometries of the *trans–trans* **A(X)**, *cis–trans* **B(X)** and *trans–cis* **C(X)** conformers of methoxy(substituted-siloxy)carbenes.[48] Computed transition-state geometries for 1,2-silyl migration $\mathbf{TS_{AD}(X)}$ and $\mathbf{TS_{BE}(X)}$ leading to *anti*-methyl silylformates **D(X)** and *syn*-methyl silylformates **E(X)**, respectively, and those for decarbonylation $\mathbf{TS_{CH}(X)}$ affording methyl silyl ethers **H(X)**, are also shown in Fig. 1. It appears that σ-electron-withdrawing substituents in the siloxycarbene conformers cause noticeable shrinkage of the ∠C6O7Si angle. In fact, good linear correlations are obtained for plots of the ∠C6O7Si angle *versus* Swain–Lupton modified Hammett substituent constants,[15,16] σ_I, as shown in Fig. 2. We note that the dependence of the ∠C6O7Si angle on σ_I is considerably greater for conformers **A(X)** and **B(X)** than it is for conformers **C(X)**, as evident from the magnitude of the slopes in Fig. 2. Also noteworthy is the fact that the dependence of the ∠C6O7Si angle on σ_I for conformers **B(X)** is slightly greater than that for conformers **A(X)** (*cf.* Fig. 2). We will address these observations later on in this discussion.

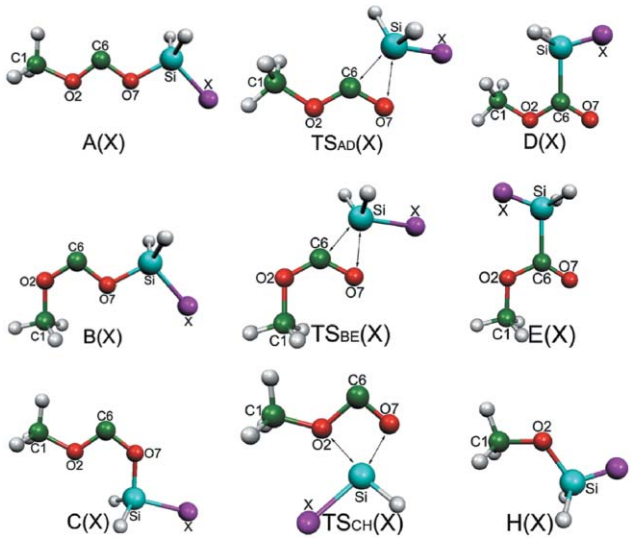

Fig. 1 Representative geometries of the *trans–trans* **A(X)**, *cis–trans* **B(X)** and *trans–cis* **C(X)** conformers of methoxy(substituted-siloxy)-carbenes, and the transition states for 1,2-silyl migration $\mathbf{TS_{AD}(X)}$ and $\mathbf{TS_{BE}(X)}$ leading to *anti*- **D(X)** and *syn*-methyl silyl formates **E(X)**, respectively, and decarbonylation $\mathbf{TS_{CH}(X)}$ leading to methyl silyl ethers **H(X)**. Corresponding pertinent geometric parameters are provided in the ESI† (*cf.* Tables S1 and S2).

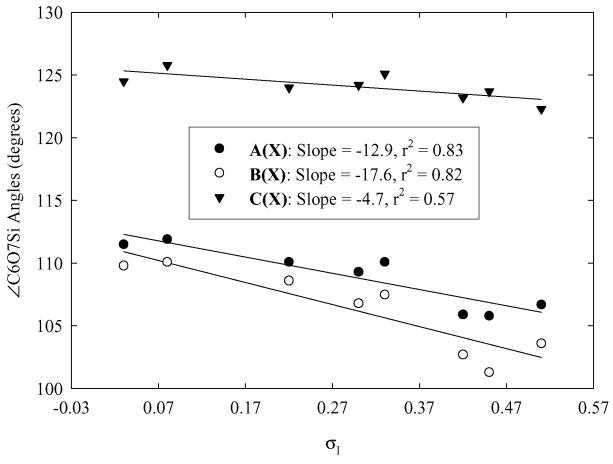

Fig. 2 Plots of the MP2/6-311+G(2d,p) ∠C6O7Si angles of the methoxy(substituted-siloxy)carbene conformers *versus* Swain–Lupton modified Hammett substituent constants.

The presence of σ-electron-withdrawing substituents in the siloxycarbene conformers also seems to give rise to slight O7–Si and O2–C6 bond shortening, as well as C6–O7 and C1–O2

bond lengthening. Fairly reasonable linear correlations are obtained for plots of the O7–Si, C6–O7, O2–C6 and C1–O2 bond lengths *versus* σ_I, as shown for conformers **A(X)** in Fig. 3. At first glance, the trends in Fig. 3 seem questionable given the shallowness of the slopes. However, reasonably good linear correlations with slopes of similar magnitudes and of the same signs are also obtained for plots of the MP2/6-311+G(2d,p) bond lengths for conformers **B(X)** and **C(X)** *versus* σ_I, and for the HF/6-311+G(2d,p) and B3LYP/6-311+G(2d,p) bond lengths for conformers **A(X)**, **B(X)** and **C(X)** *versus* σ_I, suggesting that the observed trends are real.

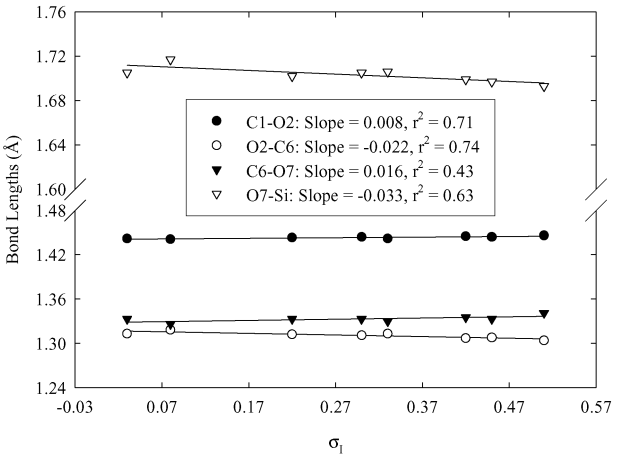

Fig. 3 Plots of the MP2/6-311+G(2d,p) bond lengths of conformers **A(X)** of methoxy(substituted-siloxy)carbenes *versus* Swain–Lupton modified Hammett substituent constants.

Let us now consider the changes in geometry in the transition states for 1,2-silyl migration and decarbonylation relative to the parent siloxycarbene conformers. In regards to 1,2-silyl migration, the ∠C6O7Si angle (*cf.* Fig. 1) shrinks from the 101.3 to 111.9° range in **A(X)** and **B(X)** to the 68.1 to 79.6° range in $\mathbf{TS_{AD}(X)}$ and $\mathbf{TS_{BE}(X)}$ based on MP2/6-311+G(2d,p) calculations. At the same time, the O7–Si bond lengthens from the 1.693 to 1.723 Å range in **A(X)** and **B(X)** to the 1.834 to 1.970 Å range in $\mathbf{TS_{AD}(X)}$ and $\mathbf{TS_{BE}(X)}$, while the C6–O7 bond shortens from the 1.326 to 1.352 Å range in **A(X)** and **B(X)** to the 1.271 to 1.301 Å range in $\mathbf{TS_{AD}(X)}$ and $\mathbf{TS_{BE}(X)}$. In addition, the planarity of $\mathbf{TS_{AD}(X)}$ and $\mathbf{TS_{BE}(X)}$ suggests that silyl migration occurs in the plane containing the carbene lone pair. These observations are consistent with nucleophilic attack by the carbene C6 lone pair at silicon, along with O7–Si bond dissociation and C6–O7 double-bond formation. Regarding decarbonylation, the ∠C6O7Si angle shrinks from the 122.3 to 125.8° range in **C(X)** to the 102.4 to 105.0° range in $\mathbf{TS_{CH}(X)}$. Simultaneously, the O2–C6 and O7–Si bonds lengthen from the 1.330 to 1.338 Å and 1.696 to 1.722 Å ranges, respectively, in **C(X)** to the 1.445 to 1.477 Å and 1.879 to 1.951 Å ranges in $\mathbf{TS_{CH}(X)}$, while the C6–O7 bond shortens from the 1.318 to 1.338 Å range in **C(X)** to the 1.248 to 1.266 Å range in $\mathbf{TS_{CH}(X)}$. These geometric changes are in keeping with nucleophilic attack by the methoxy oxygen O2 at silicon, together with O2–C6 and O7–Si bond dissociation, and C6–O7 triple-bond formation.

Electronic structure

In light of the above observations that the presence of σ-electron-withdrawing substituents in the methoxy(substituted-siloxy)carbene conformers shortens the O7–Si and O2–C6 bonds, and lengthens the C6–O7 and C1–O2 bonds, we decided to examine the dependence of the bond critical point[46] (BCP) electronic densities $\rho_b(r)$ on σ_I. It turns out that $\rho_b(r)$ increases for the O7–Si and O2–C6 bonds and decreases for the C6–O7 and C1–O2 bonds with stronger σ-electron-withdrawing substituents, in accordance with the observed changes in bond lengths. Moreover, fairly good linear correlations are obtained for plots of $\rho_b(r)$ *versus* σ_I, as shown for conformers **A(X)** in Fig. 4.

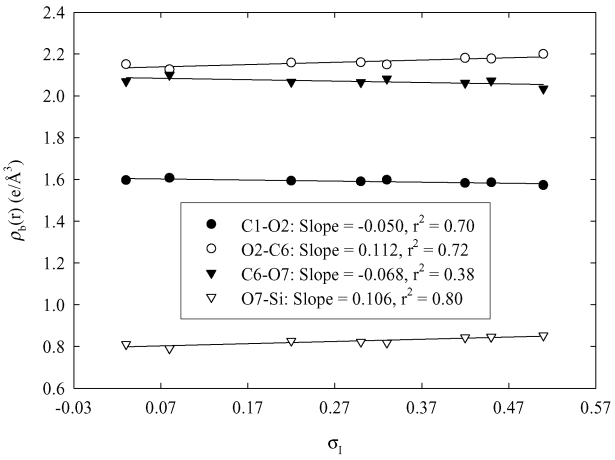

Fig. 4 Plots of the MP2/6-311+G(2d,p) BCP electronic densities *versus* Swain–Lupton modified Hammett substituent constants for conformers **A(X)** of methoxy(substituted-siloxy)carbenes.

The geometric changes in the transition states for 1,2-silyl migration and decarbonylation relative to the parent siloxycarbene conformers are also reflected in the BCP electronic densities $\rho_b(r)$. For 1,2-silyl migration, the shrinkage of the ∠C6O7Si angles in $\mathbf{TS_{AD}(X)}$ and $\mathbf{TS_{BE}(X)}$ relative to **A(X)** and **B(X)** generally results in weak C6–Si bond formation with low $\rho_b(r)$ values ranging from 0.494 to 0.610 *e* Å^{-3} at the MP2/6-311+G(2d,p) level. Simultaneously, $\rho_b(r)$ decreases for the lengthening O7–Si bonds and increases for the shortening C6–O7 bonds. In general, $\rho_b(r)$ for the O7–Si bonds decreases from values in the 0.780 to 0.853 *e* Å^{-3} range in **A(X)** and **B(X)** to values in the 0.509 to 0.589 *e* Å^{-3} range in $\mathbf{TS_{AD}(X)}$ and $\mathbf{TS_{BE}(X)}$, whereas $\rho_b(r)$ for the C6–O7 bonds increases from values in the 1.976 to 2.082 *e* Å^{-3} range in **A(X)** and **B(X)** to values in the 2.270 to 2.461 *e* Å^{-3} range in $\mathbf{TS_{AD}(X)}$ and $\mathbf{TS_{BE}(X)}$. Similarly for decarbonylation, the shrinkage of the ∠C6O7Si angle in $\mathbf{TS_{CH}(X)}$ relative to **C(X)** is accompanied by weak O2–Si bond formation with $\rho_b(r)$ values in the range 0.351 to 0.474 *e* Å^{-3}. At the same time, $\rho_b(r)$ decreases for the lengthening O2–C6 and O7–Si bonds, while it increases for the shortening C6–O7 bonds. In fact, $\rho_b(r)$ values for the O2–C6 bond ranging from 2.013 to 2.062 *e* Å^{-3} and for the O7–Si bond ranging from 0.769 to 0.830 *e* Å^{-3} in **C(X)** decrease to the 1.357 to 1.560 *e* Å^{-3} range and to the 0.469 to 0.555 *e* Å^{-3} range, respectively, in $\mathbf{TS_{CH}(X)}$. These features are in keeping with nucleophilic attack by the methoxy oxygen O2 at silicon, along with O2–C6 and O7–Si bond dissociation, and C6–O7 'triple-bond' formation.

Natural bond orbital (NBO) analysis[43] was carried out to further shed light onto the changes in electronic structure in going from the parent methoxy(substituted-siloxy)carbene conformers to the transition states for 1,2-silyl migration and decarbonylation. The electronic structure of the siloxycarbene conformers is most likely a hybrid of the three resonance structures shown in Scheme 3. NBO analysis was performed using

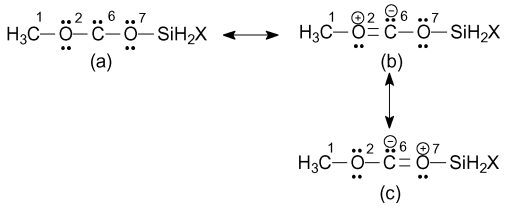

Scheme 3

Table 1 HF/6-311+G(2d,p)//MP2/6-311+G(2d,p) NBO stabilization energies in the parent siloxycarbene conformers and the transition states for 1,2-silyl migration[a]

X	σ_I	% Lewis structure	$n(\pi)_{O2} \rightarrow p_{C6}$	$n(\pi)_{O7} \rightarrow p_{C6}$	$n(\sigma)_{C6} \rightarrow \sigma^*_{O7\text{-}Si}$
A(X)					
H	0.03	98.8	107.87	92.77	6.64
NH_2	0.08	98.8	104.21	97.23	5.01
CCH	0.22	98.9	109.05	92.62	6.80
SH	0.30	98.9	109.55	92.59	7.43
OH	0.33	98.8	107.58	94.82	5.28
Cl	0.42	98.9	112.68	92.87	8.74
F	0.45	98.8	112.02	94.78	6.91
CN	0.51	98.9	116.10	88.61	8.94
B(X)					
H	0.03	98.7	110.77	86.50	7.01
NH_2	0.08	98.8	106.87	91.05	5.36
CCH	0.22	98.8	112.10	86.29	7.27
SH	0.30	98.9	114.11	85.32	9.15
OH	0.33	98.8	110.41	89.56	6.01
Cl	0.42	98.8	115.96	88.44	10.68
F	0.45	98.7	115.28	91.91	9.31
CN	0.51	98.8	119.38	84.13	10.63
TS_{AD}(X)					
H	0.03	97.7	103.23	185.85	77.12
NH_2	0.08	98.0	102.62	167.80	59.80
CCH	0.22	97.9	103.85	194.05	81.26
SH	0.30	98.1	107.27	176.66	69.71
OH	0.33	97.9	103.99	183.11	66.09
Cl	0.42	97.9	104.65	214.41	76.62
F	0.45	97.7	102.19	221.90	71.20
CN	0.51	97.9	109.49	198.51	86.36
TS_{BE}(X)					
H	0.03	97.5	108.44	168.72	73.39
NH_2	0.08	98.1	107.46	150.41	54.11
CCH	0.22	98.0	109.15	176.90	79.49
SH	0.30	98.2	112.59	157.94	64.18
OH	0.33	98.0	109.00	164.01	60.68
Cl	0.42	98.0	110.03	196.33	75.26
F	0.45	97.8	108.72	194.85	68.56
CN	0.51	97.9	115.15	180.39	84.73

[a] The σ_I values are Swain–Lupton modified Hammett substituent constants[15,16] for σ-electron-withdrawing substituents. Stabilization energies are in kcal mol^{-1} and were estimated by second-order NBO perturbation-energy analysis of HF/6-311+G(2d,p) wave functions generated for MP2/6-311+G(2d,p) optimized geometries.[49] % Lewis structure is the percentage of the total electronic density accounted for by the resonance-structure representation in Scheme 3(a).

the resonance-structure description shown in Scheme 3(a) for the wave functions of the parent siloxycarbene conformers and the transition states for 1,2-silyl migration and decarbonylation. As evident from Tables 1 and 2, this resonance-structure description (or Lewis structure representation) accounts for more than 98.7% of the total electronic density of the parent carbene conformers and at least 97.5% of that of the transition states for 1,2-silyl migration and decarbonylation.

The O2 and O7 atoms of conformers **A(X)**, **B(X)** and **C(X)** each have an in-plane σ-type lone-pair NBO, hereafter denoted as $n(\sigma)_{O2}$ and $n(\sigma)_{O7}$, and an out-of-plane π-type lone-pair NBO, henceforth denoted as $n(\pi)_{O2}$ and $n(\pi)_{O7}$. Fig. 5 shows these NBOs for the *trans–trans* conformer of methoxy(siloxy)carbene **A(H)**. The stabilization energies that arise from $n(\pi)_{O2} \rightarrow p_{C6}$ and $n(\pi)_{O7} \rightarrow p_{C6}$ delocalization (or π-back donation) in the carbene conformers (where p_{C6} represents the out-of-plane "vacant" carbene p orbital on C6), estimated by second-order NBO perturbation-energy analysis,[43] clearly indicate that the O2–C6 and C6–O7 bonds have considerable double-bond character (*cf.* Tables 1 and 2). For 1,2-silyl migration, the stabilization energies that arise from the $n(\sigma)_{C6} \rightarrow \sigma^*_{O7\text{-}Si}$ interaction depicted in Scheme 4(a) and $n(\pi)_{O7} \rightarrow p_{C6}$ back donation, increase dramatically in going from conformers **A(X)** and **B(X)** to **TS_{AD}(X)** and **TS_{BE}(X)**, respectively (*cf.* Table 1). This is consistent with nucleophilic attack by the carbene C6 lone pair at Si, in concert with C6–O7 double-bond formation. In addition, the stabilization energies that result from $n(\pi)_{O2} \rightarrow p_{C6}$ back donation in conformers **A(X)** and **B(X)** decrease only slightly

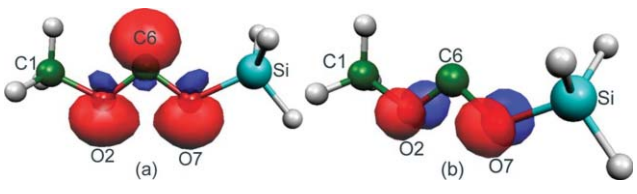

Fig. 5 Plots of (a) the in-plane σ-type lone-pair NBOs on the O2, C6 and O7 atoms and (b) the out-of-plane π-type lone-pair NBOs on the O2 and O7 atoms of conformer **A(H)** of methoxy(siloxy)carbene obtained from NBO analysis of the HF/6-311+G(2d,p) wave function.

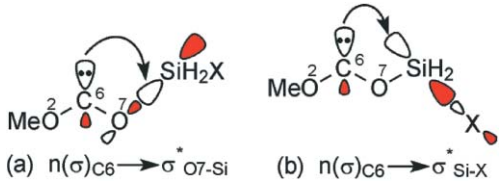

Scheme 4

Table 2 HF/6-311+G(2d,p)//MP2/6-311+G(2d,p) NBO stabilization energies in the parent siloxycarbene conformers and the transition states for decarbonylation[a]

X	% Lewis structure	$n(\pi)_{O2} \rightarrow p_{C6}$	$n(\pi)_{O7} \rightarrow p_{C6}$	$n(\sigma)_{c6} \rightarrow \sigma^*_{O7-Si}$
C(X)				
H	98.8	91.44	94.26	3.75
NH_2	98.8	89.36	97.82	2.74
CCH	98.9	91.11	93.75	3.84
SH	99.0	91.68	92.61	3.81
OH	98.8	90.74	94.53	2.82
Cl	99.0	91.46	91.15	4.04
F	98.9	90.67	92.34	3.15
CN	98.9	92.54	88.73	4.72
TS_{CH}(X)				
H	98.3	31.80	182.92	64.50
NH_2	98.4	38.98	170.20	50.59
CCH	98.5	31.17	186.58	66.20
SH	98.6	35.00	175.48	59.75
OH	98.4	34.06	182.03	58.56
Cl	98.7	37.72	161.59	58.57
F	98.5	38.65	162.02	53.36
CN	98.5	26.91	189.53	74.26

[a] Stabilization energies are in kcal mol^{-1} and were estimated by second-order NBO perturbation-energy analysis of HF/6-311+G(2d,p) wave functions generated for MP2/6-311+G(2d,p) optimized geometries.[49] % Lewis structure is the percentage of the total electronic density accounted for by the resonance-structure representation in Scheme 3(a).

in **TS_{AD}(X)** and **TS_{BE}(X)**, respectively, suggesting that π-back donation from O2 to C6 helps to stabilize the transition states for 1,2-silyl migration. In regards to decarbonylation, the stabilization energies due to the $n(\sigma)_{O2} \rightarrow \sigma^*_{O7-Si}$ interaction depicted in Scheme 5(a) increase tremendously in **TS_{CH}(X)** relative to **C(X)** as can be seen from Table 2, consistent with nucleophilic attack by the methoxy oxygen O2 at Si. As well, the stabilization energies due to $n(\pi)_{O2} \rightarrow p_{C6}$ back donation decrease significantly, indicative of the loss of double-bond character from the dissociating O2–C6 bond, while the stabilization energies that result from $n(\pi)_{O7} \rightarrow p_{C6}$ back donation increase considerably, consistent with C6–O7 'triple-bond' formation.

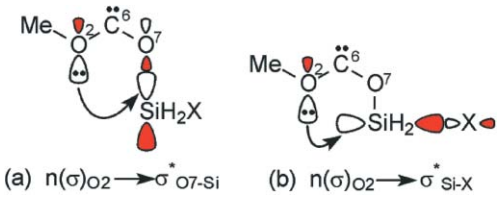

Scheme 5

Table 3 summarizes the changes in atomic charges in going from the parent carbene conformers to the transition states for 1,2-silyl migration and decarbonylation. For 1,2-silyl migration, there is significant negative and positive charge buildup at Si and O7, respectively, while there is slight negative and positive charge buildup at C6 and O2, respectively, in **TS_{AD}(X)** and **TS_{BE}(X)** relative to **A(X)** and **B(X)**. These findings are consistent with nucleophilic attack by the carbene C6 lone pair at silicon, together with C6–O7 double-bond formation and some $n(\pi)_{O2} \rightarrow p_{C6}$ back donation that facilitates stabilization of the transition states. The slight negative charge buildup at C6 suggests that the loss of charge density by C6 *via* the $n(\sigma)_{C6} \rightarrow \sigma^*_{O7-Si}$ interaction associated with nucleophilic attack by C6 at Si, is slightly less than the gain in charge density by C6 *via* the $n(\pi)_{O7} \rightarrow p_{C6}$ interaction associated with C6–O7 double-bond formation and $n(\pi)_{O2} \rightarrow p_{C6}$ back donation. In regards to decarbonylation, modest negative and positive charge developments are observed at Si and C6, respectively, while significant negative and positive charge developments are observed at O2 and O7, respectively, in **TS_{CH}(X)** relative to **C(X)**. These findings are consistent with nucleophilic attack by the methoxy oxygen O2 at Si, together with O2–C6 bond dissociation and C6–O7 triple-bond formation. The significant negative charge buildup at O2 suggests that the loss of charge density by O2 *via* the $n(\sigma)_{O2} \rightarrow \sigma^*_{O7-Si}$ interaction for nucleophilic attack by O2 at Si is considerably less than the gain in charge density by O2 *via* the weakening of the $n(\pi)_{O2} \rightarrow p_{C6}$ interaction. Similarly, the modest negative charge depletion at C6 suggests

Table 3 Changes in MP2/6-311+G(2d,p) NPA atomic charges in the transition states relative to the parent carbene conformers[a]

X	C1	O2	C6	O7	Si
TS_{AD}(X) relative to **A(X)**					
H	0.0002	0.0214	−0.0073	0.1822	−0.1939
NH_2	0.0009	0.0235	−0.0036	0.1593	−0.1619
CCH	0.0005	0.0228	−0.0034	0.1968	−0.2159
SH	0.0007	0.0243	−0.0032	0.1846	−0.1873
OH	0.0008	0.0226	−0.0085	0.1836	−0.2194
Cl	0.0003	0.0188	−0.0129	0.2285	−0.2331
F	0.0003	0.0159	−0.0190	0.2319	−0.2542
CN	0.0005	0.0217	−0.0006	0.2098	−0.2270
TS_{BE}(X) relative to **B(X)**					
H	0.0034	0.0243	−0.0226	0.1708	−0.1751
NH_2	0.0029	0.0249	−0.0139	0.1436	−0.1443
CCH	0.0049	0.0257	−0.0219	0.1861	−0.1972
SH	0.0040	0.0250	−0.0229	0.1679	−0.1873
OH	−0.0385	0.0840	−0.0488	0.1462	−0.1757
Cl	0.0064	0.0211	−0.0359	0.2128	−0.2038
F	0.0065	0.0183	−0.0346	0.2023	−0.2180
CN	0.0058	0.0232	−0.0211	0.1941	−0.1982
TS_{CH}(X) relative to **C(X)**					
H	0.0034	−0.1272	0.0531	0.1079	−0.0668
NH_2	0.0066	−0.0905	0.0204	0.1243	−0.0539
CCH	0.0041	−0.1095	0.0217	0.1486	−0.0666
SH	0.0051	−0.1039	0.0226	0.1384	−0.0678
OH	0.0058	−0.1101	0.0221	0.1353	−0.0757
Cl	0.0033	−0.0972	0.0260	0.1290	−0.0610
F	0.0071	−0.0927	0.0205	0.1284	−0.0924
CN	0.0030	−0.1252	0.0309	0.1585	−0.0645

[a] Obtained from NBO analysis. HF/6-311+G(2d,p) and B3LYP/6-311+G(2d,p) atomic charges are available in the ESI.†

that the decrease in charge density by C6 caused by the weakening $n(\pi)_{O2} \rightarrow p_{C6}$ interaction is slightly greater than the gain in charge density by C6 *via* the strengthening $n(\pi)_{O7} \rightarrow p_{C6}$ interaction in **TS_{CH}(X)** relative to **C(X)**.

Hammett free-energy relationships

The Hammett free-energy relationship for rate data is given by eqn. (1), where k_X and k_H are rate constants for the substituted and un-substituted (parent) compounds, and σ and ρ are the Hammett substituent and reaction constants, respectively. This expression can be re-written in terms of Gibbs free energies as eqn. (2), where ΔG_{TS} and $\Delta G^{H}{}_{TS}$ are the Gibbs free-energy barriers for the substituted and parent compounds.

$$\log\left(\frac{k_X}{k_H}\right) = \sigma\rho \quad (1)$$

$$\Delta G_{TS} = \Delta G^{H}{}_{TS} - 2.303RT\,\sigma\rho \quad (2)$$

Computed Gibbs free-energy (ΔG_{TS}) and enthalpy (ΔH_{TS})-barriers for 1,2-silyl migration in conformers **A(X)** and **B(X)** *via* **TS_{AD}(X)** and **TS_{BE}(X)**, respectively, and for decarbonylation of conformers **C(X)** *via* **TS_{CH}(X)** are given in Table 4. Hammett plots of ΔG_{TS} *versus* Swain–Lupton modified Hammett substituent constants, σ_I,[15,16] for 1,2-silyl migration and decarbonylation are shown in Figs. 6 and 7, respectively.

In regards to 1,2-silyl migration in conformers **A(X)** and **B(X)**, fairly reasonable linear correlations are obtained for Hammett plots of ΔG_{TS} *versus* σ_I, as can be seen in Fig. 6. In fact, the correlation seems to improve with higher levels of theory, which presumably yield more accurate relative Gibbs free energies. The Hammett plots clearly show that the Gibbs free-energy barriers are lowered by σ-electron-withdrawing substituents. This lowering of the Gibbs free-energy barriers is most likely due to the fact that σ-electron-withdrawing substituents stabilize the sizeable negative charge accumulation at Si in **TS_{AD}(X)** and **TS_{BE}(X)** that accompanies nucleophilic attack by the carbene lone pair at silicon (*cf.* Table 3). The relatively large positive Hammett ρ values (*cf.* Fig. 6) suggest that 1,2-silyl migration

Table 4 Gibbs free-energy (ΔG_{TS}) and enthalpy (ΔH_{TS}) barriers for 1,2-silyl migration and decarbonylation in methoxy(substituted-siloxy)carbenes[a]

	B3LYP		MP2	
X	ΔG_{TS}	ΔH_{TS}	ΔG_{TS}	ΔH_{TS}
TS_{AD}(X) for 1,2-silyl migration				
H	10.6	9.9	9.0	8.4
NH_2	10.3	9.5	8.9	7.9
CCH	10.7	9.9	8.6	7.9
SH	8.8	7.6	7.1	5.9
OH	8.8	7.5	7.2	6.0
Cl	7.4	7.0	6.0	5.4
F	6.0	6.0	5.0	4.6
CN	7.8	7.1	5.9	5.2
TS_{BE}(X) for 1,2-silyl migration				
H	7.4	7.3	6.2	6.0
NH_2	8.5	7.5	7.0	6.0
CCH	7.5	7.4	6.0	5.5
SH	6.0	4.7	4.9	2.4
OH	6.3	5.7	4.9	3.7
Cl	4.3	3.9	2.9	2.6
F	3.4	2.9	2.1	1.6
CN	3.5	4.1	2.8	2.5
TS_{CH}(X) for decarbonylation				
H	17.3	17.9	15.9	16.4
NH_2	16.5	15.8	13.7	13.2
CCH	18.3	18.5	15.6	15.7
SH	16.2	15.6	13.5	12.9
OH	17.3	16.5	14.4	13.9
Cl	16.6	15.9	13.9	13.2
F	15.5	15.0	13.5	13.1
CN	17.2	17.0	14.2	14.2

[a] Obtained with the 6-311+G(2d,p) basis set. Values of ΔG_{TS} and ΔH_{TS} are in kcal mol^{-1} at 298.15 K and 1.0 atm. Gibbs free-energy barriers are the difference in Gibbs free energy between the transition states and their parent carbene conformers, while the enthalpy barriers are the enthalpy difference between the transition states and their parent carbene conformers.

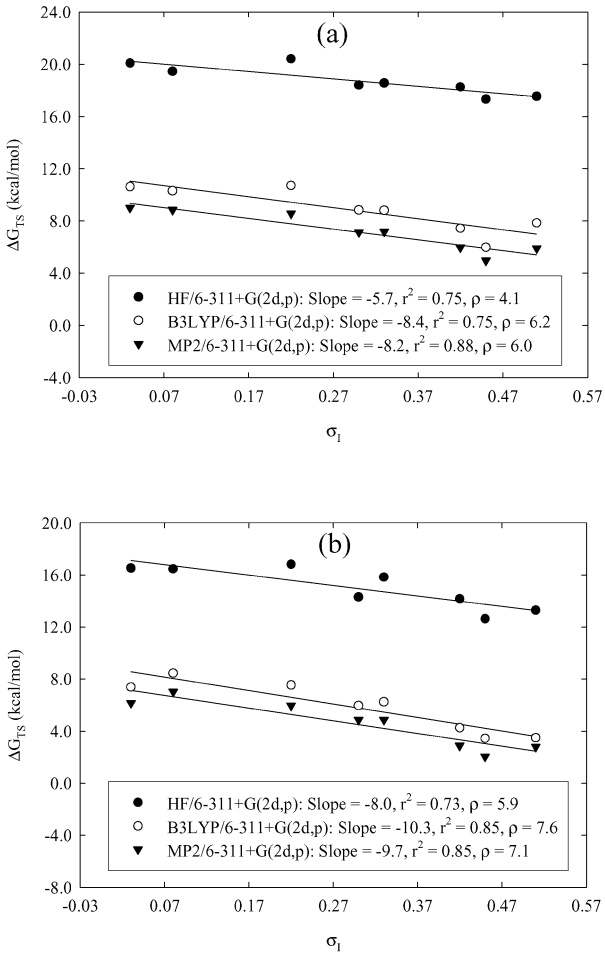

Fig. 6 Hammett plots of ΔG_{TS} *versus* σ_I for 1,2-silyl migration in (a) conformers **A(X)** and (b) conformers **B(X)** of methoxy(substituted-siloxy)carbenes. Values of ρ are Hammett reaction constants.

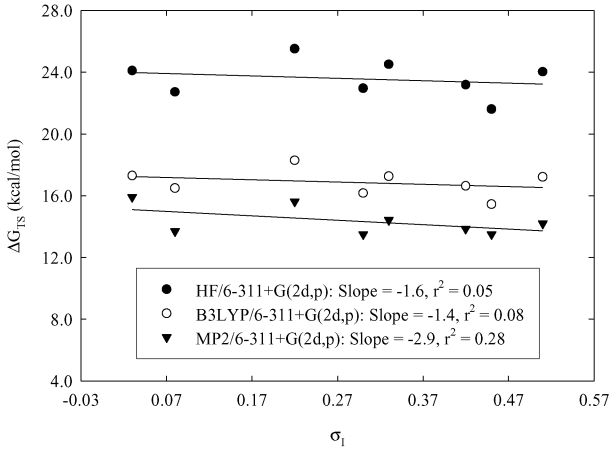

Fig. 7 Hammett plots of ΔG_{TS} *versus* σ_I for decarbonylation of conformers **C(X)** of methoxy(substituted-siloxy)carbenes.

in conformers **A(X)** and **B(X)** is quite sensitive to the presence of σ-electron-withdrawing substituents on the silyl moiety, with slightly greater sensitivity for 1,2-silyl migration in conformers **B(X)**. In regards to decarbonylation of conformers **C(X)**, although it appears from the Hammett plots in Fig. 7 that the Gibbs free-energy barriers are lowered slightly by σ-electron-withdrawing substituents, the correlations between ΔG_{TS} and σ_I are poor. These observations suggest that the Gibbs free-energy barriers are quite insensitive to the presence of σ-electron-withdrawing substituents, which is most likely due to the fact that stabilization of the meagre negative charge buildup at Si in $\mathbf{TS_{CH}(X)}$ by σ-electron-withdrawing substituents is not as meaningful as stabilization of the more substantial negative charge buildup at Si in $\mathbf{TS_{AD}(X)}$ and $\mathbf{TS_{BE}(X)}$ (*cf.* Table 3).

Role of negative hyperconjugation

In order to assess the role of negative hyperconjugation in 1,2-silyl migration and decarbonylation of methoxy(substituted-siloxy)carbenes, we investigated the relationship between activation enthalpies and stabilization energies due to the pertinent hyperconjugative interactions in the parent siloxycarbene conformers. In the case of 1,2-silyl migration in conformers **A(X)** and **B(X)** involving front-side nucleophilic attack by the carbene C6 lone pair at silicon, the pertinent hyperconjugative interactions are the $n(\sigma)_{C6} \rightarrow \sigma^*_{O7\text{–}Si}$ and $n(\sigma)_{C6} \rightarrow \sigma^*_{Si\text{–}X}$ interactions depicted in Scheme 4. For decarbonylation of conformers **C(X)** involving front-side nucleophilic attack by the methoxy oxygen O2 at silicon, the relevant hyperconjugative interactions are the $n(\sigma)_{O2} \rightarrow \sigma^*_{O7\text{–}Si}$ and $n(\sigma)_{O2} \rightarrow \sigma^*_{Si\text{–}X}$ interactions depicted in Scheme 5. Stabilization energies that arise from these hyperconjugative interactions, obtained from NBO analysis of HF/6-311+G(2d,p) wave functions at MP2/6-311+G(2d,p) optimized geometries[49] are collected in Table 5. Stabilization energies due to $n(\sigma)_{C6} \rightarrow RY^*_{Si}$ and $n(\sigma)_{O2} \rightarrow RY^*_{Si}$ interactions (where RY^*_{Si} denotes Rydberg NBOs on silicon) are also included in Table 5.

As mentioned earlier, σ-electron-withdrawing substituents in the methoxy(substituted-siloxy)carbene conformers seem to cause ∠C6O7Si angle shrinkage, O7–Si and O2–C6 bond shortening, and C6–O7 and C1–O2 bond lengthening (*cf.* Figs. 2 and 3). In addition, $\rho_b(r)$ increases for the O7–Si and O2–C6 bonds, and decreases for the C6–O7 and C1–O2 bonds, as the σ-electron-withdrawing ability of substituents increases (*cf.* Fig. 4). The ∠C6O7Si angle shrinkage that accompanies the increase in the σ-electron-withdrawing ability of substituents is most likely due to stronger $n(\sigma)_{C6} \rightarrow \sigma^*_{O7\text{–}Si}$ and $n(\sigma)_{C6} \rightarrow \sigma^*_{Si\text{–}X}$ hyperconjugation in conformers **A(X)** and **B(X)** (*cf.* Scheme 4), and $n(\sigma)_{O2} \rightarrow \sigma^*_{O7\text{–}Si}$ and $n(\sigma)_{O2} \rightarrow \sigma^*_{Si\text{–}X}$ hyperconjugation in the **C(X)** conformers (*cf.* Scheme 5). In fact, reasonable linear correlations are obtained for plots of the ∠C6O7Si angle *versus* the total stabilization energy $E^{(tot)}_{stab}$ due to the relevant hyperconjugative interactions, as shown for conformers **A(X)** in Fig. 8. We also noted earlier that the dependence of the ∠C6O7Si angle on σ_I is considerably larger in conformers **A(X)** and **B(X)** than in conformers **C(X)**, while the dependence in conformers **B(X)** is slightly larger than that in conformers **A(X)**. These observations are consistent with the total stabilization energies $E^{(tot)}_{stab}$ due to the pertinent hyperconjugative interactions given in Table 5, where those for **B(X)** are slightly larger than those for **A(X)**, and much larger than those for **C(X)**.

The O7–Si and O2–C6 bond shortening in the siloxycarbene conformers most likely arises from a strengthening of the $n(\sigma)_{O7} \rightarrow \sigma^*_{Si\text{–}X}$ and $n(\sigma)_{O2} \rightarrow \sigma^*_{C6\text{–}O7}$ negative hyperconjugation depicted in Schemes 6(a) and (c), respectively, with stronger σ-electron-withdrawing substituents, while the C6–O7 and C1–O2 bond lengthening probably results from a weakening of $n(\sigma)_{O7} \rightarrow \sigma^*_{O2\text{–}C6}$ and $n(\sigma)_{O2} \rightarrow \sigma^*_{C1\text{–}H}$ hyperconjugation depicted in Schemes 6(b) and (d), respectively. The strengthening of $n(\sigma)_{O7} \rightarrow \sigma^*_{Si\text{–}X}$ hyperconjugation by σ-electron-withdrawing substituents apparently results in a weakening of $n(\sigma)_{O7} \rightarrow \sigma^*_{O2\text{–}C6}$ and $n(\sigma)_{O2} \rightarrow \sigma^*_{C1\text{–}H}$ hyperconjugation, and a strengthening of $n(\sigma)_{O2} \rightarrow \sigma^*_{C6\text{–}O7}$ hyperconjugation. In other words, σ-electron-withdrawing substituents seem to cause an increase in $n(\sigma)_{O7} \rightarrow \sigma^*_{Si\text{–}X}$ charge transfer (hyperconjugation), which consequently reduces $n(\sigma)_{O7} \rightarrow \sigma^*_{O2\text{–}C6}$ charge transfer, resulting

Table 5 HF/6-311+G(2d,p)//MP2/6-311+G(2d,p) NBO stabilization energies in the methoxy(substituted-siloxy)carbene conformers[a]

X	$n(\sigma)_{C6} \rightarrow \sigma^*_{O7\text{–}Si}$	$n(\sigma)_{C6} \rightarrow \sigma^*_{Si\text{–}X}$	$n(\sigma)_{C6} \rightarrow RY^*_{Si}$	$E^{(tot)}_{stab}$
A(X)				
H	5.32	2.05	1.97	9.33
NH_2	3.94	2.08	4.99	11.01
CCH	5.40	2.64	5.72	13.75
SH	5.78	3.12	4.06	12.96
OH	4.18	2.18	4.22	10.58
Cl	6.70	4.17	6.29	17.16
F	5.38	3.33	5.71	14.42
CN	6.97	3.50	5.18	15.65
B(X)				
H	5.44	2.51	1.92	9.87
NH_2	4.02	2.66	4.34	11.03
CCH	5.57	3.23	2.55	11.35
SH	6.88	3.75	6.28	16.91
OH	4.51	3.07	4.39	11.97
Cl	7.70	5.80	7.62	21.12
F	6.87	5.42	7.91	20.19
CN	8.03	4.92	6.10	19.05
C(X)				
	$n(\sigma)_{O2} \rightarrow \sigma^*_{O7\text{–}Si}$	$n(\sigma)_{O2} \rightarrow \sigma^*_{Si\text{–}X}$	$n_{O2} \rightarrow RY^*_{Si}$	$E^{(tot)}_{stab}$
H	3.31	2.11	0.00	5.42
NH_2	2.39	2.09	0.00	4.47
CCH	3.37	2.44	0.00	5.81
SH	3.31	2.56	0.00	5.86
OH	2.47	2.03	0.00	4.50
Cl	3.51	2.80	0.00	6.31
F	2.76	2.29	0.00	5.04
CN	4.11	2.95	0.00	7.06

[a] Stabilization energies are in kcal mol^{-1} and were obtained from NBO analysis of HF/6-311+G(2d,p) wave functions generated for MP2/6-311+G(2d,p) optimized geometries[49] by deletion of the appropriate Fock matrix elements. $E^{(tot)}_{stab}$ is the total stabilization energy that arises from $n(\sigma)_{C6} \rightarrow \sigma^*_{O7\text{–}Si}$, $n(\sigma)_{C6} \rightarrow \sigma^*_{Si\text{–}X}$ and $n(\sigma)_{C6} \rightarrow RY^*_{Si}$ interactions in conformers **A(X)** and **B(X)**, and from the $n(\sigma)_{O2} \rightarrow \sigma^*_{O7\text{–}Si}$ and $n(\sigma)_{O2} \rightarrow \sigma^*_{Si\text{–}X}$ interactions in conformers **C(X)**. HF/6-311+G(2d,p) and B3LYP/6-311+G(2d,p) stabilization energies are available in the ESI.†

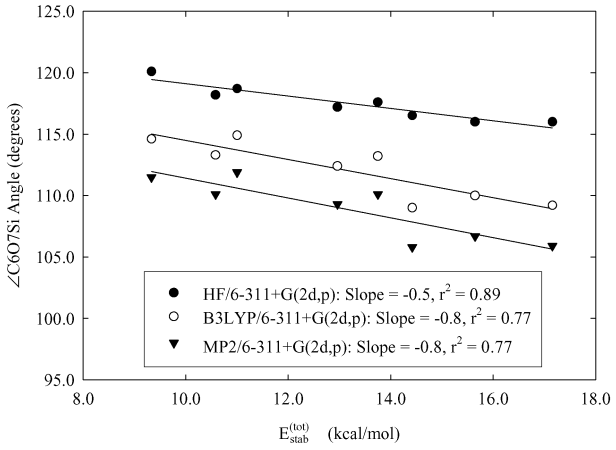

Fig. 8 Dependence of the ∠C6O7Si angle on the total HF/6-311+G(2d,p)//MP2/6-311+G(2d,p) stabilization energies $E^{(tot)}_{stab}$ due to $n_{C6} \rightarrow \sigma^*_{O7\text{–}Si}$, $n_{C6} \rightarrow \sigma^*_{Si\text{–}X}$ and $n_{C6} \rightarrow RY^*_{Si}$ hyperconjugation in conformers **A(X)** of methoxy(substituted-siloxy)carbenes.

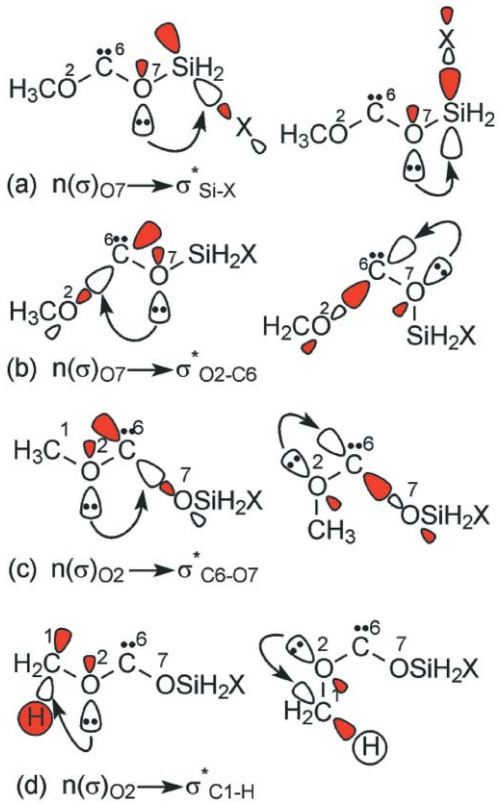

Scheme 6

in O7–Si bond shortening and C6–O7 bond lengthening. The C6–O7 bond lengthening, which implies greater bond polarization, lowers the σ^*_{C6-O7} orbital energy, consequently resulting in stronger $n(\sigma)_{O2} \rightarrow \sigma^*_{C6-O7}$ hyperconjugation and O2–C6 bond shortening. Finally, the increase in $n(\sigma)_{O2} \rightarrow \sigma^*_{C6-O7}$ charge transfer reduces $n(\sigma)_{O2} \rightarrow \sigma^*_{C1-H}$ charge transfer, which results in a weakening of the C1–O2 bond. As a matter of fact, the bond lengths are found to decrease linearly with increasing stabilization energies due to the relevant hyperconjugative interactions. This can be seen, for example, from plots of the O7–Si and C6–O7 bond lengths *versus* E_{stab} due to $n(\sigma)_{O7} \rightarrow \sigma^*_{Si-X}$ and $n(\sigma)_{O7} \rightarrow \sigma^*_{O2-C6}$ hyperconjugation, respectively, for conformers **A(X)** of the siloxycarbenes shown in Fig. 9.

It is evident from the activation enthalpies in Table 4 that 1,2-silyl migration in conformers **A(X)** and **B(X)** *via* $\mathbf{TS_{AD}(X)}$ and $\mathbf{TS_{BE}(X)}$, respectively, is considerably more favorable than decarbonylation of conformers **C(X)** *via* $\mathbf{TS_{CH}(X)}$. This can be primarily attributed to the fact that $n(\sigma)_{C6} \rightarrow \sigma^*_{O7-Si}$ and $n(\sigma)_{C6} \rightarrow \sigma^*_{Si-X}$ negative hyperconjugation in conformers **A(X)** and **B(X)** (*cf.* Scheme 4) is generally stronger than the corresponding $n(\sigma)_{O2} \rightarrow \sigma^*_{O7-Si}$ and $n(\sigma)_{O2} \rightarrow \sigma^*_{Si-X}$ interactions in conformers **C(X)** (*cf.* Scheme 5), as evident from the total stabilization energies $E^{(tot)}_{stab}$ listed in Table 5. The stronger $n(\sigma)_{C6} \rightarrow \sigma^*_{O7-Si}$ and $n(\sigma)_{C6} \rightarrow \sigma^*_{Si-X}$ hyperconjugative interactions in conformers **A(X)** and **B(X)** compared to the $n(\sigma)_{O2} \rightarrow \sigma^*_{O7-Si}$ and $n(\sigma)_{O2} \rightarrow \sigma^*_{Si-X}$ hyperconjugative interactions in the **C(X)** conformers primarily arise from the fact that the $n(\sigma)_{C6}$ orbital energies are higher than the $n(\sigma)_{O2}$ orbital energies (*cf.* Table 6). In addition, the closer proximity of the C6 and Si atoms in conformers **A(X)** and **B(X)** compared to the O2 and Si atoms in conformers **C(X)** (*cf.* Fig. 1) facilitates $n(\sigma)_{C6} \rightarrow \sigma^*_{O7-Si}$ and $n(\sigma)_{C6} \rightarrow \sigma^*_{Si-X}$ hyperconjugation, as well as $n(\sigma)_{C6} \rightarrow RY^*_{Si}$ hyperconjugation.

It is also apparent from the activation enthalpies in Table 4 that 1,2-silyl migration in conformers **B(X)** is slightly more favorable than that in their **A(X)** counterparts. This is primarily due to the smaller $n(\sigma)_{C6} \rightarrow \sigma^*_{O7-Si}$ and $n(\sigma)_{C6} \rightarrow \sigma^*_{Si-X}$ orbital-energy gaps in the **B(X)** conformers, which result from higher $n(\sigma)_{C6}$ orbital energies, and to a lesser extent lower σ^*_{O7-Si} and

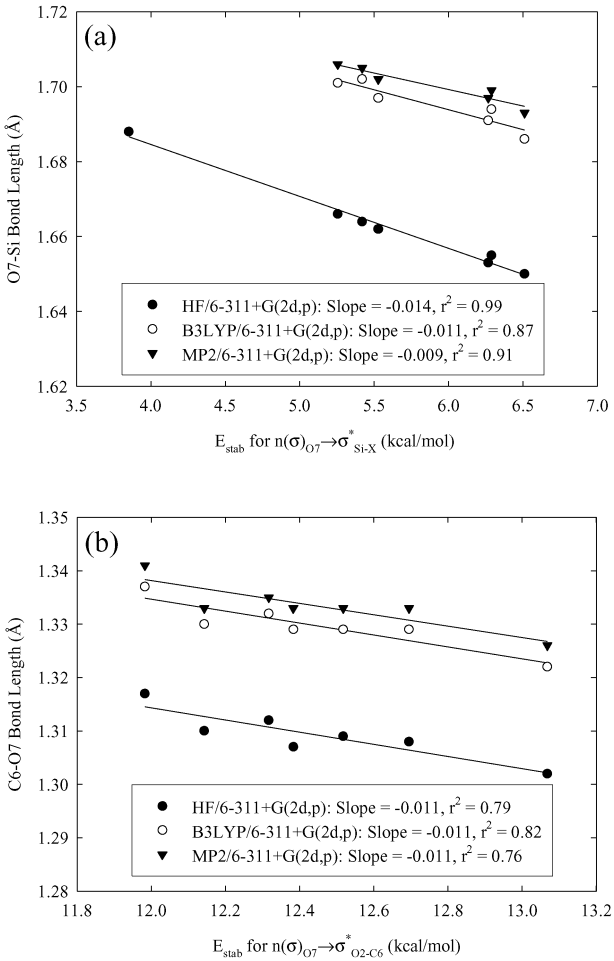

Fig. 9 Plots of (a) the O7–Si bond length and (b) the C6–O7 bond length *versus* HF/6-311+G(2d,p)//MP2/6-311+G(2d,p) NBO stabilization energies E_{stab} due to negative hyperconjugation in conformers **A(X)**. Note that one point (**X** = H) was omitted from regression analysis of the HF data, and two points (**X** = H, NH_2) from the B3LYP and MP2 data for the plots in (a), while one data point (**X** = OH) was omitted from the regression analysis for each plot in (b).

σ^*_{Si-X} orbital energies (*cf.* Table 6). Apparently, since the $n(\sigma)_{O2}$ orbital is antiperiplanar to the $n(\sigma)_{C6}$ orbital in conformers **A(X)** (*cf.* Scheme 7), interaction between these non-bonding orbitals is essentially non-existent. In contrast, the $n(\sigma)_{O2}$ orbital is synperiplanar to the $n(\sigma)_{C6}$ orbital in conformers **B(X)**, which

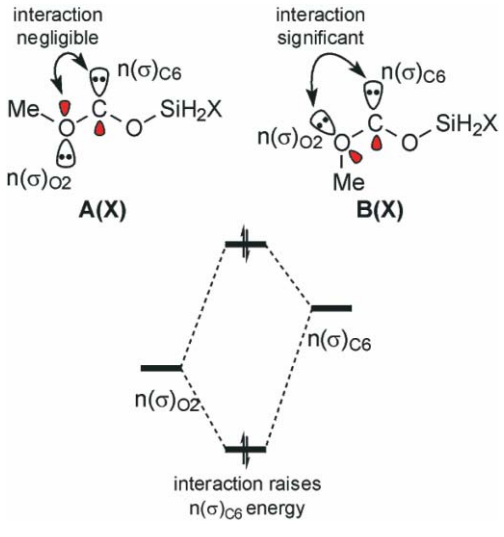

Scheme 7

Table 6 HF/6-311+G(2d,p)//MP2/6-311+G(2d,p) NBO energies and polarization coefficients for the ground-state conformers of methoxy(substituted-siloxy)carbenes[a]

X	$n(\sigma)_{C6}$	σ^*_{O7-Si}	$c_{(O7)}$[b]	$c_{(Si)}$[b]	σ^*_{Si-X}	$c_{(Si)}$	$c_{(X)}$[c]
A(X)							
H	−0.5111	0.3623	0.3720	−0.9282	0.3979	0.7897	−0.6135
NH_2	−0.5037	0.3873	0.3650	−0.9310	0.4742	0.9041	−0.4273
CCH	−0.5119	0.3798	0.3736	−0.9276	0.4820	0.8643	−0.5030
SH	−0.5141	0.3485	0.3715	−0.9284	0.3058	0.8333	−0.5528
OH	−0.5127	0.3966	0.3633	−0.9317	0.4534	0.9260	−0.3776
Cl	−0.5203	0.3518	0.3711	−0.9286	0.3137	0.8725	−0.4886
F	−0.5221	0.3953	0.3627	−0.9319	0.4239	0.9400	−0.3411
CN	−0.5309	0.3546	0.3919	−0.9200	0.4250	0.8486	−0.5290
B(X)							
H	−0.4920	0.3506	0.3674	−0.9301	0.3951	0.7910	−0.6119
NH_2	−0.4840	0.3768	0.3604	−0.9328	0.4731	0.9049	−0.4256
CCH	−0.4929	0.3699	0.3687	−0.9295	0.4780	0.8650	−0.5018
SH	−0.4960	0.3422	0.3656	−0.9308	0.2986	0.8349	−0.5504
OH	−0.4928	0.3854	0.3585	−0.9335	0.4492	0.9264	−0.3764
Cl	−0.4999	0.3380	0.3653	−0.9309	0.3103	0.8737	−0.4864
F	−0.5010	0.3800	0.3561	−0.9345	0.4215	0.9406	−0.3394
CN	−0.5110	0.3426	0.3712	−0.9285	0.4213	0.8632	−0.5049
C(X)							
	$n(\sigma)_{O2}$	σ^*_{O7-Si}	$c_{(O7)}$[b]	$c_{(Si)}$[b]	σ^*_{Si-X}	$c_{(Si)}$[c]	$c_{(X)}$[c]
H	−0.8180	0.3436	0.3800	−0.9250	0.4010	0.7885	−0.6151
NH_2	−0.8123	0.3732	0.3714	−0.9285	0.4756	0.9032	−0.4292
CCH	−0.8210	0.3619	0.3823	−0.9241	0.4849	0.8632	−0.5049
SH	−0.8233	0.3331	0.3790	−0.9254	0.3069	0.8319	−0.5549
OH	−0.8211	0.3814	0.3700	−0.9290	0.4546	0.9252	−0.3795
Cl	−0.8312	0.3381	0.3797	−0.9251	0.3148	0.8709	−0.4915
F	−0.8324	0.3824	0.3707	−0.9288	0.4231	0.9391	−0.3435
CN	−0.8414	0.3376	0.3871	−0.9220	0.4270	0.8608	−0.5089

[a] NBO energies are in atomic units and were obtained from NBO analysis of HF/6-311+G(2d,p) wave functions for MP2/6-311+G(2d,p) optimized geometries.[49] [b] Polarization coefficients $c_{(O7)}$ and $c_{(Si)}$ are those of the σ^*_{O7-Si}. [c] Polarization coefficients $c_{(Si)}$ and $c_{(X)}$ are those of the σ^*_{Si-X}. HF/6-311+G(2d,p) and B3LYP/6-311+G(2d,p) NBO energies are available in the ESI.†

maximizes interaction and consequently raises the $n(\sigma)_{C6}$ orbital energy (*cf.* Scheme 7). This means that the α-effect,[6] which refers to the increase in the nucleophilicity of a nucleophilic site when it is adjacent to lone-pair-carrying atoms, is at a minimum in conformers **A(X)** and at a maximum in conformers **B(X)**. On the other hand, the lower σ^*_{O7-Si} and σ^*_{Si-X} orbital energies in conformers **B(X)** relative to their **A(X)** counterparts most likely arise from greater polarization of the O7–Si and Si–X bonds as a result of differences in the orientation and magnitude of the net molecular dipole moments between these two types of carbene conformers. In fact, the polarization coefficients on the electronegative O7 and the electropositive Si atoms of the σ^*_{O7-Si} orbital in conformers **B(X)** are indeed slightly smaller and larger, respectively, than those in the corresponding conformers **A(X)** (*cf.* Table 6), indicative of the greater polarization of the O7–Si bond in conformers **B(X)**. Similarly, the polarization coefficients of the σ^*_{Si-X} orbitals are larger and smaller on the electropositive Si and electronegative X atoms, respectively, in conformers **B(X)** than in the corresponding conformers **A(X)** (*cf.* Table 6), again consistent with greater polarization of the Si–X bond in conformers **B(X)**.

Plots of activation enthalpies ΔH_{TS} for 1,2-silyl migration in conformers **A(X)** and **B(X)** *versus* total stabilization energies $E^{(tot)}_{stab}$ due to $n(\sigma)_{C6} \rightarrow \sigma^*_{O7-Si}$, $n(\sigma)_{C6} \rightarrow \sigma^*_{Si-X}$ and $n(\sigma)_{C6} \rightarrow RY^*_{Si}$ hyperconjugation are shown in Fig. 10. Similarly, plots of ΔH_{TS} for decarbonylation of conformers **C(X)** *versus* $E^{(tot)}_{stab}$ due to $n(\sigma)_{O2} \rightarrow \sigma^*_{O7-Si}$ and $n(\sigma)_{O2} \rightarrow \sigma^*_{Si-X}$ hyperconjugation are shown in Fig. 11. For 1,2-silyl migration, ΔH_{TS} decreases linearly with increasing $E^{(tot)}_{stab}$, suggesting that the activation enthalpies are lowered by a strengthening of the pertinent hyperconjugative interactions in conformers **A(X)** and **B(X)** (*cf.* Fig. 10). This confirms that negative hyperconjugation is indeed important in determining the ease of 1,2-silyl migration. In regards to decarbonylation of conformers **C(X)**, there seems to be no correlation between ΔH_{TS} and $E^{(tot)}_{stab}$ (*cf.* Fig. 11). Apparently, the changes in ΔH_{TS} as a function of $E^{(tot)}_{stab}$ are too small to establish an accurate measure of the true relationship between these two quantities. This can only be established by the inclusion of more data points. Of course, the plots in Fig. 11 could also simply mean that ΔH_{TS} for decarbonylation of conformers **C(X)** is absolutely independent of $n(\sigma)_{O2} \rightarrow \sigma^*_{O7-Si}$ and $n(\sigma)_{O2} \rightarrow \sigma^*_{Si-X}$ hyperconjugation.

Summary

Substituent effects and the role of negative hyperconjugation in the rearrangements of methoxy(substituted-siloxy)carbenes were investigated computationally. It was found that σ-electron-withdrawing substituents generally lower the activation barriers for 1,2-silyl migration and decarbonylation, consistent with symmetry-forbidden concerted rearrangements involving front-side nucleophilic attack by the carbene lone pair at silicon and by the methoxy oxygen at silicon, respectively. Reasonable linear Hammett correlations are obtained for 1,2-silyl migration, while those obtained for decarbonylation are poor. In addition, evidence was found suggesting that negative hyperconjugation does indeed play an important role in the rearrangements of methoxy(substituted-siloxy)carbenes; the preference for 1,2-silyl migration over decarbonylation seems to be primarily related to the fact that $n(\sigma)_{C6} \rightarrow \sigma^*_{O7-Si}$ hyperconjugation in the *trans–trans* and *cis–trans* conformers is stronger than $n(\sigma)_{O2} \rightarrow \sigma^*_{O7-Si}$ hyperconjugation in the *trans–cis* conformers of the siloxycarbenes. Moreover, the activation enthalpies for 1,2-silyl migration decrease linearly with stronger $n(\sigma)_{C6} \rightarrow \sigma^*_{O7-Si}$ and $n(\sigma)_{C6} \rightarrow \sigma^*_{Si-X}$ negative hyperconjugation. However, those for decarbonylation appear to be rather insensitive to the strength of $n(\sigma)_{O2} \rightarrow \sigma^*_{O7-Si}$ and $n(\sigma)_{O2} \rightarrow \sigma^*_{Si-X}$ hyperconjugation.

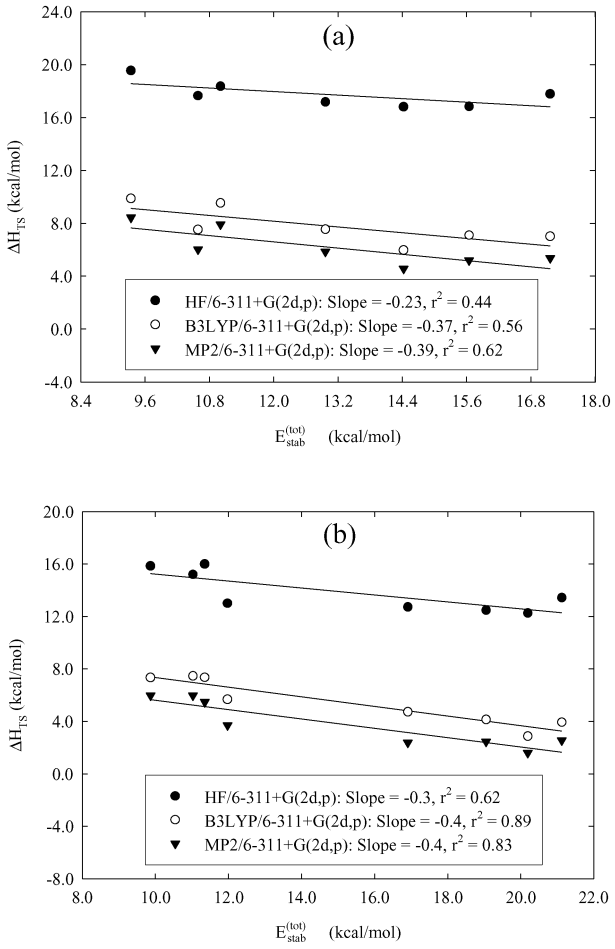

Fig. 10 Plots of the activation enthalpies for 1,2-silyl migration in (a) conformers **A(X)** and (b) conformers **B(X)** of methoxy(substituted-siloxy)carbenes *versus* the total HF/6-311+G(2d,p)//MP2/6-311+G(2d,p) stabilization energies due to $n_{C6} \rightarrow \sigma^*_{O7-Si}$, $n_{C6} \rightarrow \sigma^*_{Si-X}$ and $n_{C6} \rightarrow RY^*_{Si}$ hyperconjugation. Note that one data point (**X** = CCH) was omitted from the regression analysis for each plot in (a).

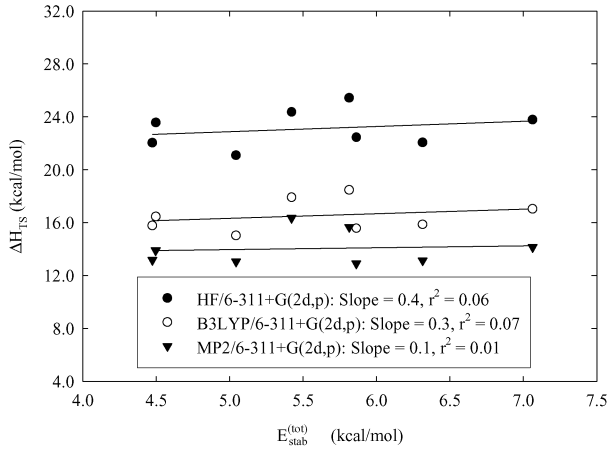

Fig. 11 Plots of the activation enthalpies for decarbonylation of conformers **C(X)** of methoxy(substituted-siloxy)carbenes *versus* total HF/6-311+G(2d,p)//MP2/6-311+G(2d,p) stabilization energies due to $n_{O2} \rightarrow \sigma^*_{O7-Si}$, $n_{O2} \rightarrow \sigma^*_{Si-X}$ and $n_{O2} \rightarrow RY^*_{Si}$ hyperconjugation.

Acknowledgements

This work was funded by research grants from the Natural Science and Engineering Research Council (NSERC) of Canada and the Fonds Québécois de la recherche sur la nature et les technologies (FQRNT-Québec). Calculations were performed at the Centre for Research in Molecular Modeling (CERMM), which was established with the financial support of the Concordia University Faculty of Arts & Science, the Ministère de l'Éducation du Québec (MEQ) and the Canada Foundation for Innovation (CFI). GHP holds a Concordia University Research Chair.

References

1 P. G. Loncke, T. A. Gadosy and G. H. Peslherbe, *Can. J. Chem.*, 2002, **80**, 302.
2 P. G. Loncke, T. A. Gadosy and G. H. Peslherbe, *ARKIVOC*, 2001, **2**, 179.
3 P. G. Loncke and G. H. Peslherbe, *J. Phys. Chem. A*, 2004, **108**, 6206.
4 R. B. Woodward and R. Hoffmann, *Angew. Chem., Int. Ed. Engl.*, 1969, **8**, 781.
5 R. Hoffmann and R. B. Woodward, *Acc. Chem. Res.*, 1968, **1**, 17.
6 I. Fleming, *Frontier Orbitals and Organic Chemical Reactions*, John Wiley & Sons, Ltd., Chichester, 1976.
7 T. L. Gilchrist, R. C. Storr, *Organic Reactions and Orbital Symmetry*, Cambridge University Press, 1979.
8 The fact that the pertinent HOMO–LUMO interactions for the 1,2-silyl migration and decarbonylation mechanisms have destabilizing antibonding components implies that the rearrangements are *symmetry-forbidden*.
9 D. T. Su and E. R. Thornton, *J. Am. Chem. Soc.*, 1978, **100**, 1872.
10 M. T. H. Liu and R. Bonneau, *J. Am. Chem. Soc.*, 1992, **114**, 3604.
11 R. A. Moss, S. Xue, W. Liu and K. Krogh-Jespersen, *J. Am. Chem. Soc.*, 1996, **118**, 12588.
12 N. Merkley and J. Warkentin, *Can. J. Chem.*, 2000, **78**, 942.
13 N. G. Rondan, K. N. Houk and R. A. Moss, *J. Am. Chem. Soc.*, 1980, **102**, 1770.
14 R. A. Moss, *Acc. Chem. Res.*, 1980, **13**, 58.
15 Hammett σ values (defined based on the ionization of benzoic acids) reflect the extent to which substituents interact with a reaction site through a combination of resonance and field/inductive effects. Generally, electron-withdrawing substituents have positive σ values, whereas electron-donating substituents have negative σ values. Since the importance of resonance and field/inductive effects vary from reaction to reaction, several modified versions of σ have been defined to more accurately reflect the significance of each effect. σ_p (based on the ionization of *p*-substituted benzoic acids) is often used for reactions where both resonance and field/inductive effects are important, σ^+ and $\sigma_R{}^+$ are usually applied to reactions in which there is direct resonance interaction between an electron-donating substituent and a cationic reaction site, and σ_I is used for reactions in which there is no resonance component.
16 C. Hansch, A. Leo and R. W. Taft, *Chem. Rev.*, 1991, **91**, 165.
17 A negative ρ value indicates that the reaction site is stabilized by electron-donating substituents.
18 We note that Moss *et al.* interpreted the negative ρ value as indicative of an anion-like shift of the acyl group to the "vacant" carbene p orbital, an interpretation that contradicted their *ab initio* findings: R. A. Moss, S. Xue, W. Liu and K. Krogh-Jespersen, *J. Am. Chem. Soc.*, 1996, **118**, 12588.
19 S. Ehrenson, R. T. C. Brownlee, R. W. Taft, in *A Generalized Treatment of Substituent Effects in the Benzene Series. A Statistical Analysis by the Dual Substituent Parameter Equation*, ed. J. A. S. Streitwieser and R. W. Taft, John Wiley & Sons, New York, 1973.
20 A. Nickon, F. Huang, R. Weglein, K. Matsuo and H. Yagi, *J. Am. Chem. Soc.*, 1974, **96**, 5264.
21 P. K. Freeman, T. A. Hardy, J. R. Balyeat and L. D. Wescott, *J. Org. Chem.*, 1977, **42**, 3356.
22 E. P. Kyba and C. W. Hudson, *J. Org. Chem.*, 1977, **42**, 1935.
23 L. S. Press and H. Shechter, *J. Am. Chem. Soc.*, 1979, **101**, 509.
24 E. P. Kyba and A. M. John, *J. Am. Chem. Soc.*, 1977, **99**, 8329.
25 E. P. Kyba, *J. Am. Chem. Soc.*, 1977, **99**, 8330.
26 H. Tomioka, T. Sugiura, Y. Masumoto, Y. Izawa, S. Inagaki and K. Iwase, *J. Chem. Soc., Chem. Commun.*, 1986, 693.
27 H. Tomioka, N. Hayashi, N. Inoue and Y. Izawa, *Tetrahedron Lett.*, 1985, **26**, 1651.
28 M. C. Pirrung and J. R. Hwu, *Tetrahedron Lett.*, 1983, **24**, 565.
29 R. Bonneau, M. T. H. Liu and M. T. Rayez, *J. Am. Chem. Soc.*, 1989, **111**, 5973.
30 J. A. LaVilla and J. L. Goodman, *J. Am. Chem. Soc.*, 1989, **111**, 6877.
31 A. E. Keating, M. A. Garcia-Garibay and K. N. Houk, *J. Am. Chem. Soc.*, 1997, **117**, 10805.
32 G. V. Shustov, M. T. H. Liu and A. Rauk, *J. Phys. Chem. A*, 1997, **101**, 2509.

33 F. Jensen, *Introduction to Computational Chemistry*, John Wiley & Sons Ltd., Chichester, 1999.
34 W. J. Hehre, L. Radom, P. v. R. Schleyer, J. A. Pople, *Ab Initio Molecular Orbital Theory*, John Wiley & Sons, New York, 1986.
35 A. D. Becke, *J. Chem. Phys.*, 1993, **98**, 5648.
36 C. Lee, W. Yang and R. G. Parr, *Phys. Rev. B*, 1988, **37**, 785.
37 M. J. Frisch, G. W. Trucks, H. B. Schlegel, G. E. Scuseria, M. A. Robb, J. R. Cheeseman, V. G. Zakrzewski, J. J. A. Montgomery, R. E. Stratmann, J. C. Burant, S. Dapprich, J. M. Millam, A. D. Daniels, K. N. Kudin, M. C. Strain, O. Farkas, J. Tomasi, V. Barone, M. Cossi, R. Cammi, B. Mennucci, C. Pomelli, C. Adamo, S. Clifford, J. Ochterski, G. A. Petersson, P. Y. Ayala, Q. Cui, K. Morokuma, D. K. Malick, A. D. Rabuck, K. Raghavachari, J. B. Foresman, J. Cioslowski, J. V. Ortiz, A. G. Baboul, B. B. Stefanov, G. Liu, A. Liashenko, P. Piskorz, I. Komaromi, R. Gomperts, R. L. Martin, D. J. Fox, T. Keith, M. A. Al-Laham, C. Y. Peng, A. Nanayakkara, C. Gonzalez, M. Challacombe, P. M. W. Gill, B. Johnson, W. Chen, M. W. Wong, J. L. Andres, C. Gonzalez, M. Head-Gordon, E. S. Replogle and J. A. Pople, *Gaussian 98, Revision A.11.4*, Gaussian, Inc., 2002.
38 H. B. Schlegel, *J. Comput. Chem.*, 1982, **3**, 214.
39 C. J. Cerjan and W. H. Miller, *J. Chem. Phys.*, 1981, **75**, 2800.
40 J. Simons, P. Jorgensen, H. Taylor and J. Ozment, *J. Phys. Chem.*, 1983, **87**, 2745.
41 A. Bannerjee, N. Adams, J. Simons and R. Shepard, *J. Phys. Chem.*, 1985, **89**, 52.
42 J. W. Ochterski, *Thermochemistry in Gaussian*, Gaussian Inc., 2000.
43 A. E. Reed, L. A. Curtiss and F. Weinhold, *Chem. Rev.*, 1988, **88**, 899.
44 E. D. Glendening, A. E. Reed, J. E. Carpenter, F. Weinhold, *NBO 3.0 Program Manual*, Theoretical Chemistry Institute and Department of Chemistry, University of Wisconsin.
45 R. F. W. Bader, *Atoms in Molecules. A Quantum Theory*, Clarendon Press, Oxford, 1990.
46 A bond critical point (BCP) is the point of minimum electronic density ρ(r) along a bond or bond path: R. F. W. Bader, *Atoms in Molecules: A Quantum Theory*, Clarendon Press, Oxford, 1990.
47 The AIMPAC suite of programs is available from Professor R. F. W. Bader, McMaster University, Canada, and from the AIMPAC website (www.chemistry.mcmaster.ca/aimpac).
48 Only carbene conformers with the Si–X bond antiperiplanar to the O2–C6 bond were considered in this work.
49 NBO only evaluates orbital energies and stabilization energies due to hyperconjugation if a well-defined one-electron effective Hamiltonian operator such as the Fock or Kohn–Sham operator is available. No such operator is available for correlated descriptions such as MP2.